International Journal of Engineering & Technology, 7 (4.25) (2018) 72-76

International Journal of Engineering & Technology

Website: www.sciencepubco.com/index.php/IJET

Research paper

Lift and Drag Performances of O-Ring Paper Plane

N. I. Ismail[1]*, Hamid Yusoff [1]*, Hazim Sharudin[1], Arif Pahmi[1], S. Suhaimi [2] & Abdul Rahman Hemdi[1]

[1]*Faculty of Mechanical Engineering, Universiti Teknologi Mara (Pulau Pinang), Kampus Permatang Pauh, 13500 Permatang Pauh, Pulau Pinang, Malaysia.*

[2]*Faculty of Mechanical Engineering, Universiti Teknologi MARA Shah Alam, 40450, Shah Alam, Selangor*

**Corresponding author E-mail: iswadi558@ppinang.uitm.edu.my*

Abstract

The O-ring paper plane is viewed as another option of paper planes that have potential to be upgraded as Micro Air Vehicle (MAV). Despite the complexity of the closed wing design, the O-Ring (OR) paper planes are easy to develop by following a certain origami technique. However, the aerodynamics performances for such closed wing design is still open to be explored before it can be upgraded for MAV usage. The aerodynamics complexity of closed wing design combined with various hoop sizing may induced complicated aerodynamics performance for OR paper planes. Thus, the objective of this research is to investigate the hoop diameters influence towards the aerodynamics performance of OR paper plane. Three different OR paper planes configurations known as OR-1, OR-2 and OR-3 have been used for comparative study. ANSYS-CFX simulation was fully utilized in this works to simulate the virtual wind tunnel on each OR paper planes configurations. The comparison works have been conducted to study the distributions of C_L, C_D and C_L/C_D on the closed wing configurations. C_L results shows that OR-3 induces 16.6% better C_L magnitude compared to OR-2 and OR-1. In fact, the OR-3 and OR-2 with larger hoop size produced better C_{Lmax} and α_{stall} performances compared to smaller hoop configuration (OR-1). The C_D performance also shows that OR-3 (with larger hoop configuration) produced at least 1.4% better $C_{D\,min}$ than the other configurations. However, the results show that OR-3 configurations has suffered from larger $C_{D\,increment}$ with at least 2% larger $C_{D\,increment}$ magnitude compared to OR-2 and OR-1. C_L/C_{Dmax} results exhibited that OR-3 induces the highest C_L/C_{Dmax} at 6.27 which is about 5.9% and 13.1% higher than OR-2 and OR-1 produced, respectively. The analysis on the low-pressure distribution area reveals that larger area of low pressure C_P found on OR-3 has been lead into better C_L magnitude for OR-3. Based on these results, one can presume that larger hoop size on OR paper planes induces higher C_L and C_L/C_D max performances due to better low-pressure C_P distributions on the wing.

Keywords: *MAV; Aerodynamics; O-Ring Paper Plane*

1. Introduction

Micro Air Vehicle (MAV) is known as a small size aircraft which is portable and specially designed to perform reconnaissance and surveillance missions. It has produce a tremendous usage in performing hazardous area, reconnaissance and indoor information gathering missions. MAV is smaller version of Unmanned Aerial Vehicle (UAV) that can also be controlled with normal flight controller system. MAV offers a lot of advantages such as portable, stealthy and lightweight[1]. Based on the MAV's sizes, it has been useful for military or civilian missions [2]. MAV is categorized based on five basic types accordingly to its wing configurations which is flapping, fixed, membrane flexible, rotary and morphing [2]. MAV has wingspan dimension and operating speeds at 15 cm and 10 m/s, respectively [3]. Based on the operating speed, MAV fall within the region of low Reynolds number range (Re ≈10,000 to 100 000). Based on the low Reynolds number regime, MAV has been exposed to large increment in drag and huge loss in aerodynamic efficiencies[4].

Paper plane is another option of fixed wing MAV that has been introduced for young ages. It is a small-scale glider that can be made from a piece of paper[5]. Paper planes can be fold into any desired shape and the size of the wingspan. Nowadays, paper plane has undergone many changes in terms of their design. One of the popular paper plane design is known as O-Ring (OR) paper plane as shown in Figure 1. OR paper plane is closed wing design which unconventional and complex wing design. Despite the complexity of the closed wing design, the OR paper planes easily made by following a certain origami technique[6]. However, the aerodynamics performances for such closed wing design is still open to be explored before it can be upgraded for MAV usage.

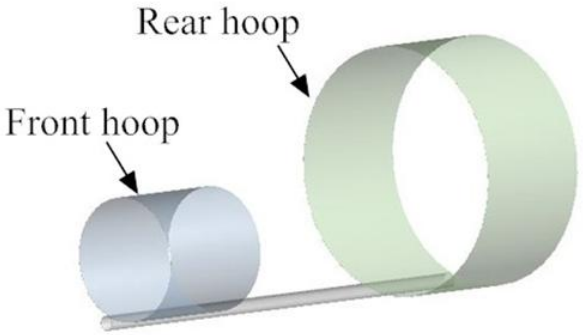

Fig 1: O-Ring paper plane

The aerodynamics complexity of closed wing design combined with various hoop sizing may induced complicated aerodynamics performance for OR paper planes. Thus, current study is conducted to investigate the lift and drag performances of OR paper planes with different ring diameter configurations. Here, three OR paper planes with different ring diameters configuration are used

for comparative study. In this investigation, ANSYS-CFX simulation is fully utilized to analyze lift and drag performances for each OR paper planes configurations. The results shall elucidate the effect of hoop diameters on the lift and drag performances of OR paper planes.

2. Methodology

The simulation works started by modelling three different configuration for O-Ring paper planes known as OR-1, OR-2 and OR-3. ANSYS-CFX simulation is fully utilized in the methodology to analyze lift and drag performances for each OR paper planes configurations. The simulation was based incompressible, steady state and 3-Dimesional model. Navier-Stokes equation (RANS) combined with Shear Stress Turbulence (SST) model are fully employed in the airflow domain.

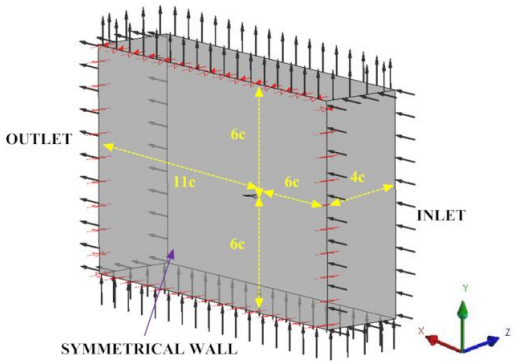

Fig 3. The boundary conditions applied on airflow domain

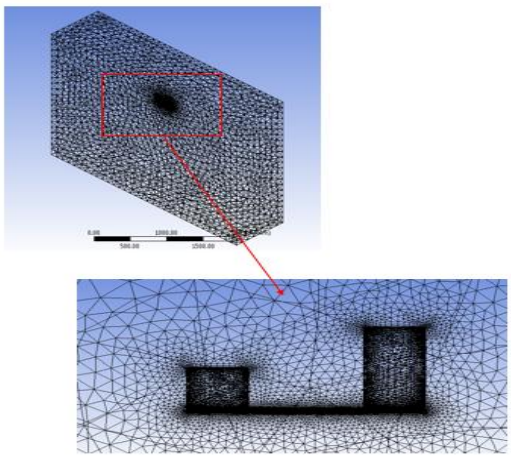

Fig 4. The mesh developed surrounding the OR model.

2.1. O-Ring Paper Plane Models

All models have common wing configurations that have smaller front hoop diameter than the rear hoop diameter as shown in Figure 1. Here, three different hoop sizing configurations were used for comparative study which known as OR-1, OR-2 and OR-3. Each configuration has different front hoop and rear hoop diameter. The minimum and maximum front hoop diameter is set at 50mm to 90mm. While the minimum and maximum rear hoop diameter is set at 100mm to 140mm. This hoop diameter dimension setup is set accordingly to MAV wingspan dimension which is below 15cm (equivalent to 150mm). However, the chord length and the overall plane size remain constant at 52mm and 200mm, respectively. To ensure each O ring paper plane is within the MAV regime, the Reynolds number operations for current OR configuration is set approximately at Re≈100,000. The detail of hoop sizing for each OR models are presented in Figure 2 and Table 1.

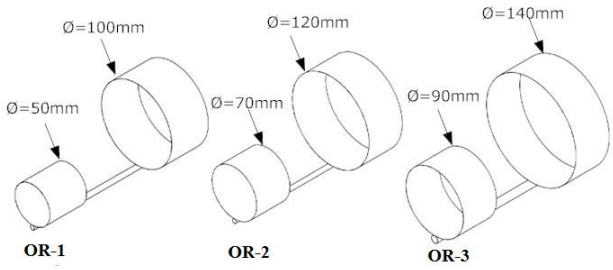

Fig 2. Different hoop sizing on each O-Ring paper plane design

Table 1: The characteristic of the 3 selected designs

OR Model	OR-1	OR-2	OR-3
Total wing area (mm^2)	7800	9880	11900
Total OR Length (mm)	200	200	200
Front diameter (mm)	50	70	90
Rear diameter (mm)	100	120	140
Chord length (mm)	52	52	52
Reynold number	99,989	99,989	99,989

2.2. Domain Sizing and Mesh Generation

ANSYS-Workbench framework is fully utilized in this works to ensure the compatibility between the CAD modelling and meshing works. The air domain was developed enclosing each model based on standard sizing as pictured in Figure 3. By manipulating the symmetrical wing design and to avoid the computational burden, the airflow domain for each model were reduced into half. Each wing part were initially united into one part in order to develop a conforming mesh characteristic in the flow domain. 3D element type with ANSYS SOLID 187 were used for the unstructured hybrid mesh. The first cell above the hoop surface was determine at $y^+ \leq 1$ to ensure the boundary layers behavior along the wing surface is sufficiently captured. The optimized mesh approximately at 727745 elements was used and built surrounding each OR configuration as shown in Figure 4. The optimum mesh obtained

based on three level of mesh independent study conducted on the same domain.

2.3. Boundary Conditions

The details of boundary conditions applied on the air domain is already shown in Figure 3. The flow vectors directions indicated the location of inlet and outlet (shown in Figure 3). To ensure the Re≈100,000 achieved at the wing chord, the inlet flow velocity was set at 29.1 m/s. The continuity and uniform flow field was assumed to filled out the air domain with zero pressure boundary condition was imposed at the outlet. To avoid the computational burden, the symmetrical wall was fully implemented and slip surface boundary conditions applied at the side walls (opposite wall of symmetrical wall). Viscous effect was captured by applying the non-slip boundary on the hoop surface. An automatic wall function is fully employed to support the viscous simulations. The tilted angle (Angle of Attack) for all OR design was varied between -10° to 40° with 2° interval. In this works, only a steady state solution with incompressible flow assumed for flow model. The airflow was solved based on RANS SST turbulent model. To ensure the reliability of solution, the simulation convergence was used with the magnitude of momentum residual was set to be below 1.0×10^{-5}. The stability in lift coefficient (C_L) and drag coeffi-

cient (C_D) magnitude was also monitored to indicate the solution convergence.

3. Result and Discussion

3.1. Lift and Drag Performance of O-Ring Paper Plane Wings

In this section, aerodynamic results based on ANSYS-CFX simulation are presented with details are given on the performances of lift coefficient (C_L), and drag coefficient (C_D). Based on C_L and C_D results, a detail study on the aerodynamic efficiency (C_L/C_D) were also conducted with view to find the best performance for all OR models. Each result presented here is based on comparative study between the model configurations. At the end of this section, high and low-pressure regions found on the OR wing surface are presented to elucidate its connection with the C_L and C_D distributions.

3.1.1. C_L Performances

The C_L performances for all OR models are presented in Figure 5. The figure shows that each OR paper plane configuration produces almost similar C_L trends throughout the angle of attack (α) increment. Each configuration produces linear increment in C_L magnitude with respect to α especially in the pre-stall angle of attack region (α before the stall angle, α_{stall}). At the beginning of C_L curves, all wing produces almost similar zero-lift-angle magnitude ($\alpha_{CL=0}$) at $\alpha_{CL=0}$=0°. This is normal indication since each wing does only has a flat wing which has similar effect to symmetrical airfoil wing condition. The C_L curve continue to increase proportionately with respect to α until it reaches at C_{Lmax} which is the peak point of C_L magnitude at α_{stall}. C_{Lmax} is the highest point of C_L magnitude before it slightly drops and plateau at the post-stall area (α after α_{stall}). Detail comparison analysis has been carried out to elucidate the different in C_L, C_{Lmax} and α_{stall} magnitude among the OR configurations. Analysis exhibited that OR-3 produced the best C_L magnitude among the configurations. OR-3 produce approximately 16.6% to 23.3% higher C_L magnitude compared to OR-2 and OR-1, respectively. Based on the C_{Lmax} magnitude, it shows that OR-3 exhibited the highest C_{Lmax} at C_{Lmax}=0.613. This value is about 6.3% at and 14.2% higher than OR-2 and OR-1 produced, respectively. The α_{stall} detail study shows that OR-2 and OR-3 produce almost similar α_{stall} magnitude at α_{stall}=30º. However, OR-1 has induced the earliest stall angle at α_{stall} =26º which is 15.4% earlier than OR-2 and OR-3 produced. Based on these results, it obviously shows that OR-3 and Or-2 with larger hoop sizing has promising advantages in producing better C_L magnitude and C_{Lmax} performance. Thus, based on these C_L results one can presume that the OR models with bigger hoop size which contribute into larger aspect ratio theoretically produces the better C_L performances.

3.1.2. C_D Performances

Figure 6 shows the drag coefficient (C_D) results for all OR paper plane configurations. The results clearly shows that each OR paper plane configurations produced almost similar and coherent C_D trend throughout the throughout the α increment. In general, the trend shows that C_D performance for each model increase with the α raise. To elucidate the difference in C_D performance, a detail comparison study has been conducted at minimum drag magnitude ($C_{D\,min}$) and the overall C_D increment ($C_{D\,increment}$) magnitude with respect to the α increment. Based on the $C_{D\,min}$ occurrence, the results exhibited that all configurations produce similarly $C_{D\,min}$ value at α =0º. However, the detail investigation reveals that that OR-3 produced the smallest $C_{D\,min}$ magnitude marked at $C_{D\,min}$ =0.01546. OR-2 has $C_{D\,min}$ at 0.0157 which is 1.4% higher than OR-3. OR-1 produce the uppermost $C_{D\,min}$ value at $C_{D\,min}$ =0.016. This $C_{D\,min}$ magnitude found in OR-1 is also 3.5% higher than the $C_{D\,min}$ magnitude of found in OR-3. Further analysis was conducted on $C_{D\,increment}$ magnitude and it shows that OR-3 produces the highest $C_{D\,increment}$ magnitude at $C_{D\,increment}$ = 22.82%. This is obviously discovered at α between 0º to 20 º. This is followed by OR-2 and OR-1 with magnitude of $C_{D\,increment}$ registered at 22.33% and 21.36%, respectively. Despite the difference found in $C_{D\,increment}$ magnitude, the overall distinction among the $C_{D\,increment}$ is still below than 2%. Based on the C_D performance, one can be presumed that bigger hoop size prompted larger drag penalty. The reason behind this condition is due to bigger surface area found in OR-3 and OR-2. This has contributed into more airflow exposure which has also lead into the greater skin drag[7].

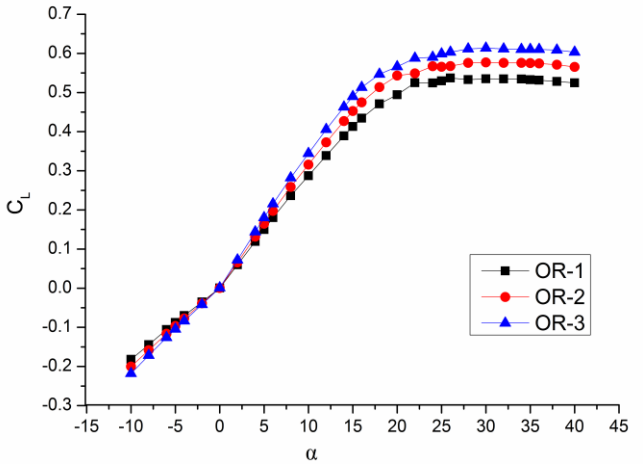

Fig. 5: The C_L performances for all OR models.

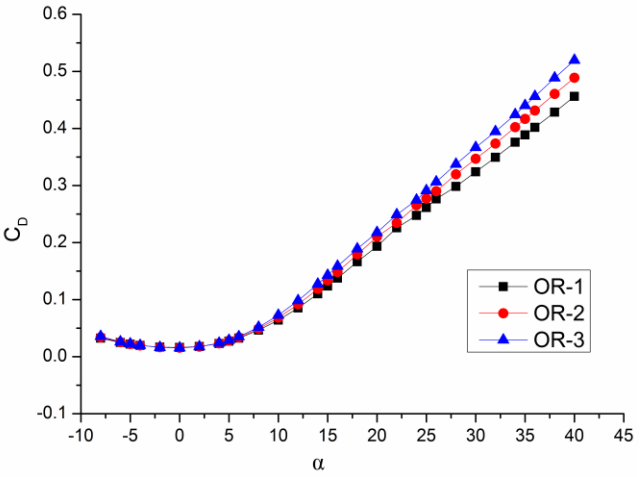

Fig. 6: The C_D performances for all O-Ring paper plane configurations.

3.1.3. C_L/C_D Performance

Figure 7 presents the aerodynamic efficiency (C_L/C_D) for all OR models. The overall trend found on the C_L/C_D curves shows that the magnitude of C_L/C_D linearly increase at the initial stages at C_L = 0.16 - 0.18. The curve reaches its peak point at the maximum aerodynamic efficiency ($C_L/C_{D\,max}$) magnitude. By taking a detail analysis on the $C_L/C_{D\,max}$ magnitude, the result exhibited that each OR models produced the $C_L/C_{D\,max}$ at α between 5º to 6º (or equivalent to C_L=0.16 ~ 0.18). After $C_L/C_{D\,max}$ reached, the C_L/C_D curve tend to reduce its magnitude. A detail study on $C_L/C_{D\,max}$ performance has elucidated the level of maximum efficiencies for every OR models. The analysis reveals that OR-3 generated the best $C_L/C_{D\,max}$ magnitude among the configurations with $C_L/C_{D\,max}$ magnitude marked at 6.27. This is followed by OR-2 and OR-1 at $C_L/C_{D\,max}$ =5.93 and $C_L/C_{D\,max}$ =5.56, respectively. Based on

these $C_L/C_{D\ max}$ performances it shows that OR-3 configuration produce about 5.9% and 13.1% better $C_L/C_{D\ max}$ magnitude compared to OR-2 and OR-1, respectively. This has been contributed by larger surface area found in OR-3 which encourage better C_L distribution which consequently produced better the $C_L/C_{D\ max}$ performance. Based on this $C_L/C_{D\ max}$ performance, one can conclude that the OR configuration with bigger hoop size enhanced $C_L/C_{D\ max}$ performances.

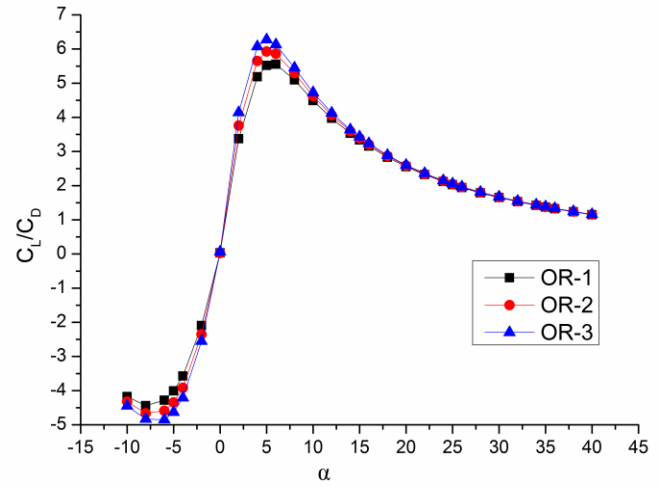

Fig. 7: The C_L/C_D performances for all O-Ring paper plane configurations.

3.6. Low Pressure Distributions on O-Ring Paper Plane

In this section, the study on the low-pressure distribution over each OR paper plane is conducted with view to elucidate the lift distribution on such wing. Figure 8 presents the low-pressure distribution for all OR paper plane configurations at at α incidence of 20º. The result is based on simulation works obtain from the ANSYS-CFX simulation. The study focused on the formation of the low-pressure ($-C_P$) contours on the wing surface (which related to the lift distribution). To clarify the difference in pressure characteristics, the result is presented at α incidence of 20º and clipped at low-pressure coefficient region ($-C_P$) particularly at $C_P < 0$ value. Higher attention has been given on the approximate area of $C_{P\ min}$ (lowest pressure coefficient, $C_{P\ min}$=-0.007661) area that highly contribute into C_L generation. The α=20º is selected since it shows the best variation of C_L distributions (Figure 5) among the configurations before stall (α_{stall}).

Based on the low-pressure distribution results as shown in Figure 8, all wing exhibits almost similar low-pressure distribution particularly on the front and rear hoop. At the front hoop, the lowest low-pressure distribution ($C_{P\ min}$=-0.007661) has been concentrated mostly on the lower side of the hoop and spread towards the middle side of front hoop. It similarly happens at the rear hoop in which the intensity of lowest pressure distribution ($C_{P\ min}$=-0.007661) has mostly found at the lower hoop side and extent to the middle and slightly on the upper side of rear hoop. Despite of the similarity in lowest pressure distributions, the approximate very low-pressure area (C_P between -0.007661 to -0.004597) is the mostly found on OR-3 design. Based on detail area analysis, 72.6% of front and rear hoop of OR-3 covered with low pressure area of C_P between -0.007661 to -0.004597. This is followed by OR-2 and OR-1 at 71.3% and 68.6%, respectively. Even though the percentage area difference is very small among the wing (below 5%), the total wing area for OR-3 is at least 21.4% larger the other configurations. Based on these results, it just clarifies the significant of higher C_L magnitude found in OR-3. The larger area of low pressure C_P found on OR-3 has translated and lead into better C_L magnitude for OR-3. The similar trend also found between OR-2 and OR-1. Larger area of low pressure C_P found on OR-2 has induced better C_L magnitude for OR-2 compared to OR-1.

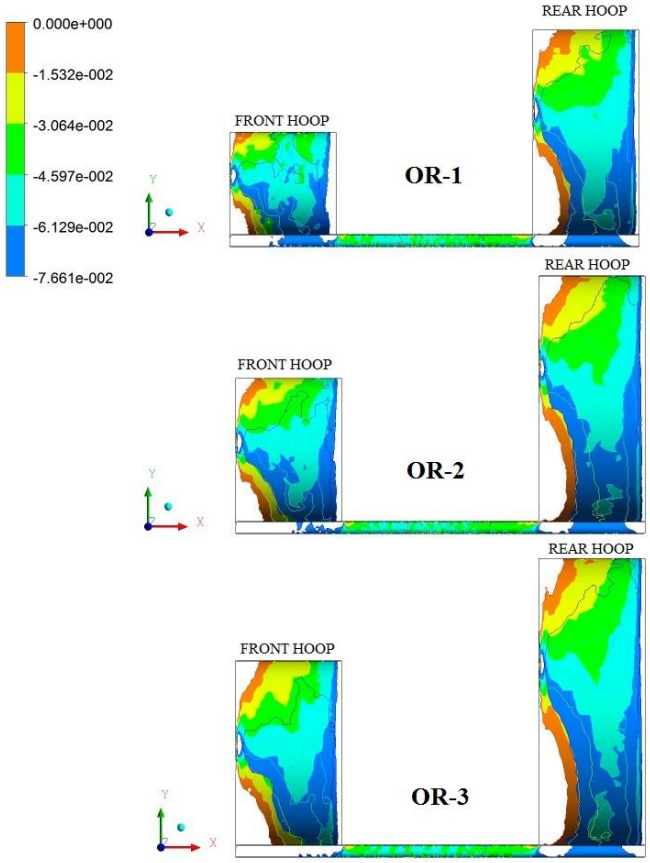

Fig. 8: The low-pressure distribution on all O-Ring paper plane wings at α = 20°.

4. Conclusion

In current work, three different OR paper plane configurations (OR-1, OR-2 and OR-3) were used in comparative study with view to find the effect of different hoop sizing. The comparison works have been conducted to study the distributions of C_L, C_D and C_L/C_D on the closed wing configurations. C_L results shows that OR-3 minimally induces about 16.6% better C_L magnitude compared to the other configurations. Furthermore, the OR paper plane configuration with bigger hoop sizes (as found in OR-3 and OR-2) produced better C_{Lmax} and α_{stall} performances than the smaller hoop configuration (OR-1). The C_D performance also shows that the OR paper plane configurations with bigger hoop configuration (OR-3) produced at least 1.4% better $C_{D\ min}$ than the other configurations. Despite the advantages shows in C_L results and $C_{D\ min}$, OR-3 configurations has suffered from larger $C_{D\ increment}$. The OR-3 configuration produces at least 2% larger $C_{D\ increment}$ magnitude than OR-2 and OR-1. Detail analysis on $C_L/C_{D\ max}$ magnitude shows that OR-3 induces the highest $C_L/C_{D\ max}$ magnitude marked at 6.27. These $C_L/C_{D\ max}$ magnitude, is about 5.9% and 13.1% higher than $C_L/C_{D\ max}$ magnitude found in OR-2 and OR-1, respectively. The detail analysis on the low-pressure distribution area on each configuration reveals that larger area of low pressure C_P found on OR-3 has been translated and lead into better C_L magnitude for OR-3 which subsequently contributed into better $C_L/C_{D\ max}$ magnitude. Based on these performances, one can presume that the OR configuration with larger hoop size produces better C_L and $C_L/C_{D\ max}$ performances but slightly suffered in C_D performances.

Acknowledgement

Authors acknowledge technical and financial support from Universiti Teknologi MARA Cawangan Pulau Pinang and the Government of Malaysia.

References

[1] H. Yu, M. Seger, and A. Malik, "Wing Frame Design and Strain Tuning for Optimum Endurance of Flexible Fixed-Wing Micro Air Vehicles," in *2018 AIAA/AHS Adaptive Structures Conference*, 2018, pp. 1–8.

[2] M. A. Tasin, N. I. Ismail, R. J. Talib, and H. Yusoff, "Enabling Concepts and Technologies for Out-Of-Plane Morphing Wing Structure : A Review," *Australian Journal of Basic and Applied Sciences*, vol. 9, no. 37, pp. 449–456, 2015.

[3] N. I. Ismail, a. H. Zulkifli, M. Z. Abdullah, M. H. Basri, and N. S. Abdullah, "Optimization of aerodynamic efficiency for twist morphing MAV wing," *Chinese Journal of Aeronautics*, vol. 27, no. 3, pp. 475–487, Jun. 2014.

[4] D. Ninian and S. M. Dakka, "Design, Development and Testing of Shape Shifting Wing Model," *Aerospace*, vol. 4, no. 52, pp. 1–24, 2017.

[5] N. B. Feng, K. Q. Mei, P. Y. Yin, and J. U. Schlüter, "On the Aerodynamics of Paper Airplanes," in *27th AIAA Applied Aerodynamics Conference*, 2009, no. June, pp. 1–16.

[6] Didier Boursin, *Origami Paper Airplanes*, 1st ed. Firefly Books, 2001.

[7] H. Yusoff, S. Suhaimi, K. M. Hyie, N. Iswadi, and A. Farhan, "Experimental Investigation of Effects of Wing Camber on Drag for a Bio-Mimic MAV Flapping Wing," *Journal of Mechanical Engineering*, vol. 5, no. 5, pp. 16–28, 2018.